Neuroscience Informatics 1 (2021) 100013

Contents lists available at ScienceDirect

Neuroscience Informatics

www.elsevier.com/locate/neuri

Original article

The DCT-CNN-ResNet50 architecture to classify brain tumors with super-resolution, convolutional neural network, and the ResNet50

Anand Deshpande [a,*], Vania V. Estrela [b], Prashant Patavardhan [c]

[a] Department of Electronics & Communication Engineering, Angadi Institute of Technology and Management, Belagavi, Karnataka, India
[b] Telecommunications Department, Federal Fluminense University, Rio de Janeiro, Brazil
[c] Department of Electronics & Communication Engineering, RV Institute of Technology and Management, Bengaluru, Karnataka, India

ARTICLE INFO

Article history:
Received 18 June 2021
Received in revised form 22 September 2021
Accepted 22 September 2021

Keywords:
Super-resolution
Convolution Neural Network
Discrete cosine transform
Brain tumor
Fusion
Image recognition

ABSTRACT

Brain tumors' diagnoses occur mainly by Magnetic resonance imaging (MRI) images. The tissue analysis methods are used to define these tumors. Nevertheless, few factors like the quality of an MRI device and low image resolution may degrade the quality of MRI images. Also, the detection of tumors in low-resolution images is challenging. A super-resolution method helps overcome this caveat. This work suggests Artificial Intelligence (AI)-based classification of brain tumor using Convolution Neural Network (CNN) algorithms is proposed to classify brain tumors using open-access datasets. This paper hiders on a novel Discrete Cosine Transform-based image fusion combined with Convolution Neural Network as a super-resolution and classifier framework that can distinguish (aka, classify) tissue as tumor and no tumor using open-access datasets. The framework's performance is analyzed with and without super-resolution method and achieved 98.14% accuracy rate has been detected with super-resolution and ResNet50 architecture. The experiments performed on MRI images show that the proposed super-resolution framework relies on the Discrete Cosine Transform (DCT), CNN, and ResNet50 (aka DCT-CNN-ResNet50) and capable of improving classification accuracy.

1. Introduction

A brain tumor that may form in the skull is characterized as abnormal and unrestrained synapses. It puts pressure on the brain and harmfully affects the health of a human being. According to the National Brain Tumor Foundation (NBTF) data, the brain tumor death rate has recently increased by nearly 200% in many countries [1–3]. Early detection and classification of tumors are vital to the research domain in biomedical imaging and, as a result, helps deliver treatment methods that increase the chances of patient survival. Magnetic resonance imaging (MRI) is the most popular imaging technique as it affords radiologists detailed information on brain tumors. But, few factors like the quality of an MRI device and low image resolution may degrade the quality of MRI images. Also, the detection of tumors in low-resolution images is challenging. Super-resolution (SR) schemes overcome this problem by crafting a high-resolution (HR) image whose expanded, and enhanced details stem from adequate processing of low-resolution (LR) images [4–6]. By augmenting the images' resolution, MRI image becomes more apparent, which helps to classify the tumor correctly. SR techniques are classified in to three methods viz. interpolation, reconstruction, and learning-based methods [7–13]. From under-sampled LR observations, the primary concern of the SR algorithm is to reconstruct HR images; it produces high-quality images from blurred, noisy, and degraded images. The advantages of the SR approach are i) costs less, ii) existing (legacy) LR imaging systems can be repurposed and still utilized without any additional hardware, and iii) flexibility.

Many approaches permit brain tumor classification like as neutrosophic set [14,15], deep neural networks [16], entropy-based [17], fully convolutional neural networks (FCNNs) [18], optimal symmetric multimodal templates, and concatenated random forests [19], deep convolutional neural network (CNN) [20], superpixel-based classification [21], transfer learning and fine-tuning [22] and many more. The author [23] proposed CNN architecture for MRI images and classified the tumor as meningioma, glioma, and pituitary with 96.56% accuracy. The author [24] proposed CNN-based brain tumor classification using a computer-assisted diagnosis (CAD) system. They performed experiments on three datasets using the CNN model, which has 18-weighted layered and achieved 94.74% accuracy. The author [25] recommended deep learning to classify brain tumors into tumor and non-tumor

* Corresponding author.
E-mail address: deshpande.anandb@gmail.com (A. Deshpande).

https://doi.org/10.1016/j.neuri.2021.100013

using more than 200 MRI images with data augmentation and achieved 89% classification accuracy.

The contributions of this paper are,

- Discrete cosine transform (DCT)-based is a novel fusion technique to fuse multiple images of MRI images. Here, the best quality patches of images are selected using the suggested method and fused in the DCT domain. The quality of the output image increases by using a consistency verification procedure.
- The second contribution is the Convolution neural network (CNN) used to super-resolve the low-resolution MRI image.
- Combining the DCT fusion, CNN SR, and ResNet50 frameworks (aka, DCT-CNN-ResNet50 architecture) within the same design gives rise to the third contribution. This is the first time appearance of the DCT-CNN-ResNet50 in research to the best of the authors' knowledge.

The paper is structured as follows. Section 2 discusses the projected framework, which contains a novel fusion technique. Section 3 discusses the results obtained using the devised system. Finally, the concluding remarks appear in Section 4.

2. DCT-CNN-ResNet50 method

The DCT-CNN-ResNet50 brain tumor detection framework appears below Fig. 1.

The proposed brain tumor classification framework contains the following blocks.

- Image extraction: The MRI images from scan sequences are extracted and have contrast adjustment by histogram technique called Histogram Equalization on Fuzzy based Improved Particle Swarm Optimization (FIPSO) [26].

In this, the details of an image are captured by smoothing and it uses Gaussian function to distribute pixel intensity to nearest pixel and blur is removed by applying Non subsampled Contourlet Transform. The dark and bright pixel values are extracted by calculating local maxima. The smoothed images are fuzzified with Takagi-Sugeno-Kang model and it provides importance to all the local maxima intervals. FIPSO algorithm is used to the minimum contrast images of MRI brain images.

- Best quality patch selection and Fusion: Instead of using a global SR algorithm, a local patch-based SR approach is used to super-resolve the MRI images. In this method, the LR image is divided into subsets of square areas. The local deformation can be avoided by employing local patches to perform SR on the MRI image. The LR images are divided into patches of size 8×8. The patches from different images, which belong to the same location, are stored in the local group. The image in this group is added with the help of a first-order derivative of the patch, generated by the Sobel filter to produce an enhanced patch. The enhanced patches in this group are fused to get a single LR image using the DCT-CNN-ResNet50 fusion method, as discussed below.

Consider image $F = \{f_{i,j}\}$ where $i = 0 \ldots N-1$ and $j = 0 \ldots M-1$ and it is divided in P number of blocks having a size of 8×8 pixels. Let $B_n = \{b_{n,k,l}\}$ be the n^{th} 8×8 block, where $n = 0..P-1; l = 0..7;\ k = 0..7$. The DCT output of block B_n be $Y_n = \{y_{n,k,l}\}$. The DCT of image F is represented as set $D = D_0, D_1, D_2 \ldots . D_{P-1}$. DCT of the R^{th} input image is represented as $D^R = D_o^R, D_1^R, D_2^R \ldots . . D_{P-1}^R$. DCT of fused image is represented as $D^F = D_o^F, D_1^F, D_2^F \ldots . . D_{P-1}^F$ and obtained by fusing the DCT coefficients of images A and B. The steps involved in the algorithm are as below.

1) Let P_n^A be the n^{th} block of image A and P_n^B be the n^{th} block of image B.
2) Obtain DCT coefficients of images A and B.

$$D_n^A = \mathrm{DCT}\left(P_n^A\right) \quad \text{and} \quad D_n^B = \mathrm{DCT}\left(P_n^B\right).$$

The actual formula for the two-dimensional DCT is shown below. The DCT is performed on an N x N square matrix of pixel values, and it yields an N x N square matrix of frequency coefficients.
The DCT [27] is calculated as below.

$$F(u,v) = \frac{2}{N} c(u)c(v) \sum_{y=0}^{N-1} \sum_{x=0}^{N-1} f(x,y) \cos\left[\frac{(2x+1)u\pi}{2N}\right] \times \cos\left[\frac{(2y+1)v\pi}{2N}\right], \tag{1}$$

where $u, v = 0, 1, \ldots, N-1$, with

$$c(u) = \begin{cases} \frac{1}{\sqrt{N}}, & \text{if } u = 0 \\ \frac{\sqrt{2}}{\sqrt{N}} 1, & \text{if } u \neq 0. \end{cases} \tag{2}$$

Here, $c(u) = c(v)$ as $N \times N$ square matrix of pixel values is used.
3) Extract AC and DC coefficients of both the blocks and mask DC coefficients to zero:

$$D_{n(0)}^A = 0 \quad \text{and} \quad D_{n(0)}^B = 0. \tag{3}$$

4) Square all AC components of the coefficients of blocks from images A and B:

$$\left[D_{n(1:63)}^A\right]^2 \quad \text{and} \quad \left[D_{n(1:63)}^B\right]^2. \tag{4}$$

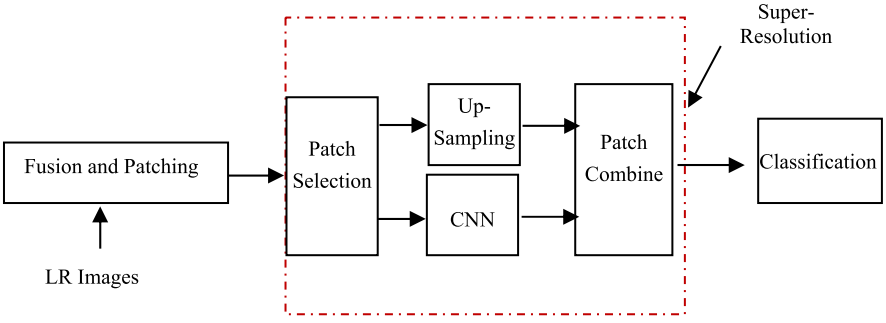

Fig. 1. DCT-CNN-ResNet50 Brain tumor classification framework.

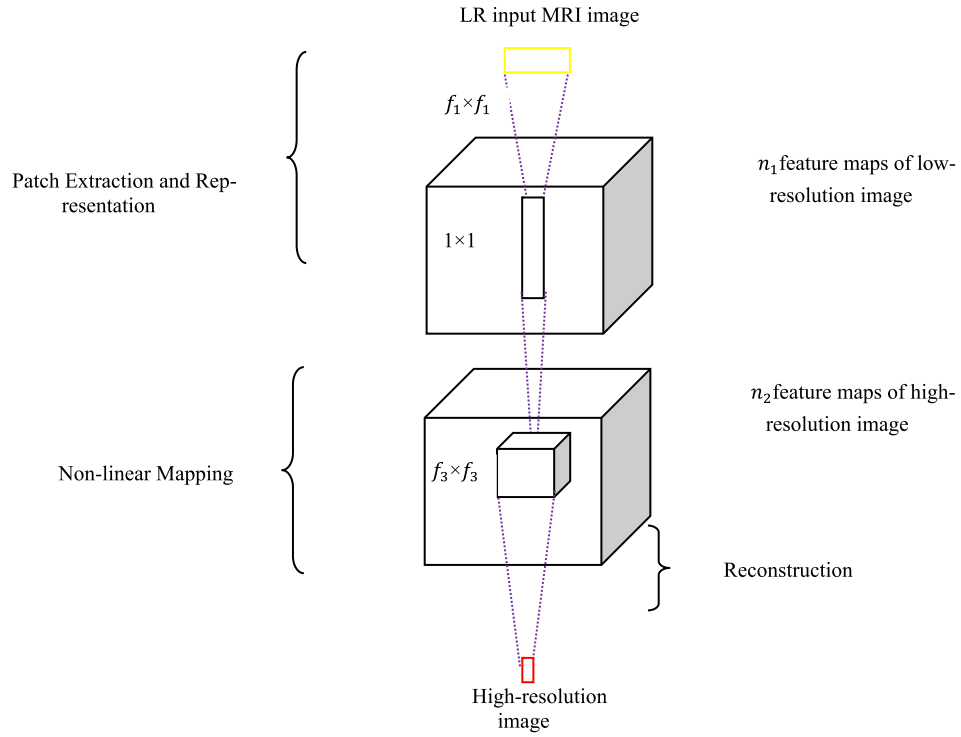

Fig. 2. Convolutional Neural Network-based Super-Resolution.

5) Add coefficients from 1 to 31 of blocks from images A and B:

$$L_n^A = D_{n(1:31)}^A \quad \text{and} \quad L_n^B = D_{n(1:31)}^B. \tag{5}$$

6) Add coefficients from 32 to 63 of blocks of images A and B:

$$H_n^A = D_{n(32:63)}^A \quad \text{and} \quad H_n^B = D_{n(32:63)}^B. \tag{6}$$

7) Calculate the quality of each block by using this equation:

$$BQ_n^A = \frac{H_n^A}{L_n^A} \quad \text{and} \quad BQ_n^B = \frac{H_n^B}{L_n^A}. \tag{7}$$

8) Compare the quality of each block to decide which block is used to construct the fused image according to this rationale:

$$\text{If } BQ_n^A > BQ_n^B, \text{ then } D_n^F = D_n^A \tag{8}$$

else

$$D_n^F = D_n^B. \tag{9}$$

9) Apply consistency verification [28] procedure to avoid erroneous selection of blocks. The consistency verification utilizes a 3 × 3 neighborhood window. In this verification process, if the center block is from image A and the blocks of image B surround it, the center block is replaced by the image B block.
10) The above steps are repeated for all P blocks to fuse DCT coefficients of multiple images into a single DCT representation of the image.
11) Apply the inverse DCT (IDCT) and fuse the DCT coefficients to reconstruct the fused image. The IDCT results from this expression:

$$f(x,y) = \frac{2}{N}\sum_{v=0}^{N-1}\sum_{u=0}^{N-1} c(u)(v)F(u,v)\cos\left[\frac{(2x+1)u\pi}{2N}\right] \times \cos\left[\frac{(2y+1)v\pi}{2N}\right], \tag{10}$$

where $x, y = 0, 1, \ldots, N-1$.

Patch Selection and super-resolution

The local patch-based SR approach is used to super-resolve the fused image. In this method, the whole image is divided into 10 × 10 size patches. The contents of the image patches are analyzed in this block by calculating the variance of each patch. If the patch variance is more than the predefined value, then the patch is sent to the CNN block for SR. If the variance is less than the predefined value, then the patch is sent to the up-sampling block. If the CNN processes the patch containing the least amount of information, then the overall processing time will increase. To avoid this, the patch which has the smallest amount of information is processed by up-sampling. This patch selection method increases the speed of the SR process.

The overview of the convolution neural network appears in Fig. 2.

The following steps carry out the super-resolution of the fused image patch.

Block I: This block is called a representation block. The strategy for image reconstruction is by getting patches and representing them by a set of pre-trained bases. This is achieved by convolving the patch with a group of filters. Overlapped patches of images are extracted and characterized by a set of pre-trained Discrete Cosine Transform bases.

Consider x as LR image. The Bicubic interpolation-based up-sampled image is X. Now, the objective is to recover from X and image $F(X)$, similar to the reference HR image X. The representation of this reasoning follows,

$$F_1(X) = \max(0, S_1 * X + V_1), \tag{11}$$

where

- V_1-n_1-dimensional vector, in which element is associated with a filter,

- S_1-Convolution filter having a size of $m \times f_1 \times f_1 \times n_1$,
- n_1-Number of filters,
- f_1-Spatial size of the filter,
- m-Number of channels.

The output has n_1 feature maps.

Block II: Non-linear mapping block. n_1-dimensional feature vectors are mapped onto n_2-dimensional feature vectors by

$$F_2(X) = \max\left(0, S_2 * F_1(Y) + V_2\right), \tag{12}$$

where,

- n_2-number of feature maps,
- V_2-n_2 dimensional vector, and
- S_2-size $n_1 \times 1 \times 1 \times n_2$

Block III-Reconstruction Block. The predicted HR patches are averaged to produce the final HR image given by

$$F(X) = S_3 * F_2(X) + V_3, \tag{13}$$

where,

- V_3-l-dimensional vector,
- S_3-size $n_2 \times f_3 \times f_3 \times k$.

In the training process, network parameters $K = (W_1, W_2, W_3, V_1, V_2, V_3)$ are required to be determined to learn the end-to-end mapping function F. These network parameters are obtained by reducing the loss between HR image X and the reconstructed images $F(X, K)$ with the assistance of this loss function

$$L(K) = \frac{1}{n}\sum_{i=1}^{n}\left\|F(x_i, K) - X_i\right\|^2, \tag{14}$$

where,

- x_i-LR image, and
- X_i-Corresponding HR image.

The loss is minimized by stochastic gradient descent with the standard back-propagation method.

Classification

A CNN categorizes the brain tumor images as Tumor or No Tumor images. CNNs require a massive quantity of data for training, but available image datasets are limited to recognize brain tumors. Due to this limitation, CNN-based brain tumor detection approaches mainly utilize pre-trained CNN models. The system is trained using Inceptionv3, AlexNet [29], GoogLeNet, VGG-16 [30], and ResNet50 [31]. The softmax layers of pre-trained networks identify images. The system is trained multiple times for all these networks using Stochastic gradient descent with momentum (SGDM) to attain the best possible trained system. While the features from the fixed pre-trained networks can be helpful in tumor classification, a more precise classifier can be trained by fine-tuning the parameters of the network.

Performance metrics

The standard performance evaluation metrics analyze the performance of the proposed framework. They are accuracy, specificity, sensitivity, precision, and the area of the receiver operating characteristic (ROC) curve and the area under a ROC Curve (AUC). The formulas for these metrics are as below.

- Accuracy: The capacity of a system to decide the type of tumor correctly:

$$\text{Accuracy} = \frac{TP + TN}{TP + TN + FP + FN}. \tag{15}$$

- Specificity: The capacity of a system to precisely identify the genuine tumor according to

$$\text{Sensitivity} = \frac{TP}{TP + TN}. \tag{16}$$

- Sensitivity: The capacity of a model to correctly classify the tumor given by

$$\text{Specificity} = \frac{TN}{TN + FP}. \tag{17}$$

- Precision: The proximity of the two measured values to each other as follows:

$$\text{Precision} = \frac{TP}{TP + FP}, \tag{18}$$

where, the parameters are TP = true positive, TN = true negative, FP = false positive, and FN = false negative, respectively.

3. Results

The validation of the proposed system effectiveness results from performing experiments on a reference image database to evaluate therapy response (RIDER) [32], having images 70,000 and NC Brain images [33]. The database contains MRI-multi-sequence images from 19 patients with glioblastoma. The total number of images in this dataset is 70,220. The image size taken is 224×224 in JPG format. For deployment and execution, the DCT-CNN-ResNet50 framework relies on MATLAB R2017 and i5 processor having 8 GB RAM. This section discusses the analysis of results obtained in three sections viz. Fusion, super-resolution, and recognition. Sample input images appear in the subsequent Fig. 3.

Fusion:

The DCT-CNN-ResNet50 system uses four normalized brain images to generate a fused image. This selection of 4 images relies on ROC curves for the fusion of 2, 4, and 6 images of Set_2, as in Fig. 4.

The Equal Error Rate (EER) is a biometric security system algorithm used to predetermine the threshold values for its false acceptance rate and its false rejection rate. From Fig. 4, it can be seen that the EER drops as the number of images increases from 1 to 4 as the availability of data is more. When the number of frames increases to more than 4, the quality of the image decreases due to poor focus, variation in illumination and or occlusion. As a result, this increases EER and degradation in the recognition performance. So, in this experiment best 4 numbers of low-resolution images are used, which are selected using the proposed fusion method to generate a fused image.

Super-resolution

The performance of the proposed system is evaluated by quality analysis [34–37], such as the peak signal-to-noise ratio (PSNR), structural similarity index matrix (SSIM), and visual information fidelity in the pixel domain (VIFP).

PSNR is the ratio between highest possible pixel value in the image and the noise power. The SSIM is measure for assessment of

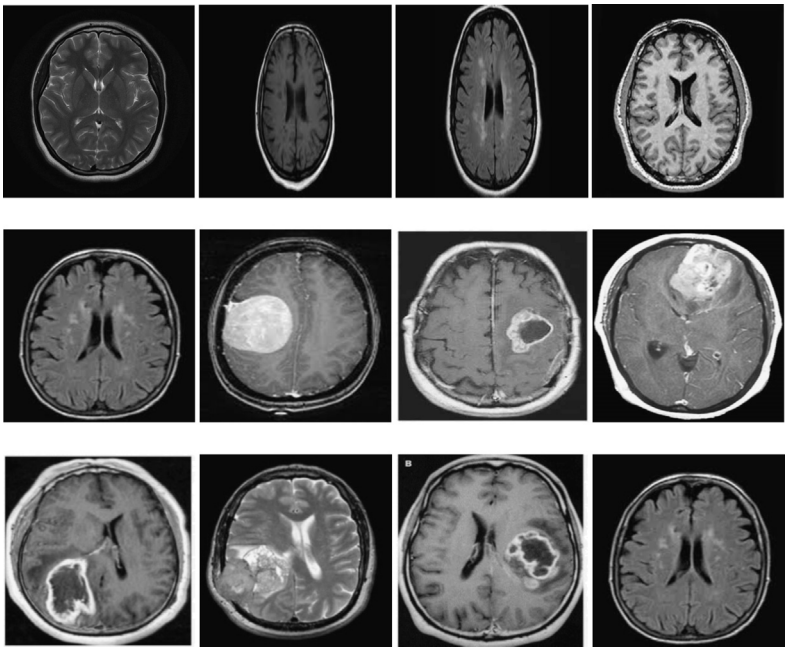

Fig. 3. Sample Input images.

Table 1
Input for Performance evaluation.

Classification Group	Images			
	Group	Training Set (60%)	Validation Set (20%)	Test Set (20%)
No Tumor	1300	1740	580	580
Tumor	1600			

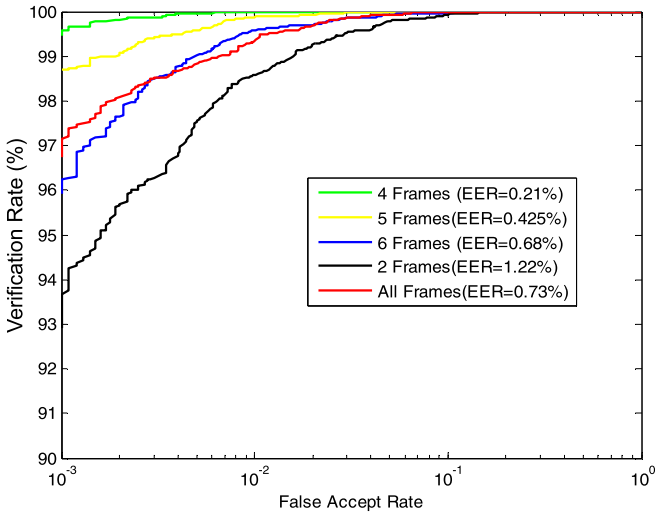

Fig. 4. ROC curves of the DCT-CNN-ResNet50 system with various numbers of images.

quality, motivated by the information that the human visual system is sensitive to distortions of the structural components. This measure assesses the changes in structural components occurred between two images. The VIFP is the statistics between first and the last stage of the visual channel at a time of no distortion, and common data among the input of distortion chunk and the output of visual system chunk. The outcome of this is a fidelity measure.

To evaluate the performance, the original high-quality images are down-sampled to get low-resolution images. Then, these LR images were super-resolved using DCT-CNN-ResNet50 and compared these super-resolved images with the original high-quality images. The images are super-resolved using the suggested method with an up-sampling factor $(\Lambda) = 2$. The size of the image patches are set to 10×10 as per the analysis shown in Fig. 5

Fig. 6 shows that the proposed system gives better quality super-resolved image compared to the conventional methods.

Table 2
Performance comparison.

S. No.	Models	Without Proposed systems		With Proposed systems	
		Accuracy (%)	AUC	Accuracy (%)	AUC
1	GoogleNet	74.81	0.801	81.67	0.816
2	AlexNet	82.13	0.854	91.84	0.883
3	VGG-16	85.37	0.868	93.06	0.929
4	**ResNet-50**	88.77	0.892	**98.14**	0.957
5	Inceptionv3	81.85	0.831	90.79	0.852

Classification

For the classification task, a total of 2900 images and images are randomly separated as training, validation, and test sets having the ratio of 60:20:20, as in Table 1.

These networks are compared in terms of accuracy and AUC obtained during the experiments. The results from the DCT-CNN-ResNet50 system and for existing CNN models surpassed other combinations investigated. For this purpose, the experiments involved pre-trained CNN models, e.g., GoogleNet, AlexNet, VGG-16, ResNet-50, and Inceptionv3, as in Table 2.

From Table 2, among the presented Pre-Trained CNNs, ResNet-50 gives the best accuracy value of 98.14% when ResNet-50 is used. Classification accuracy of 98.14% results from the ResNet-50 after 293 iterations. The framework's performance is evaluated by using sensitivity, precision metrics, accuracy, specificity, and AUC of the ROC curve, as in Table 3.

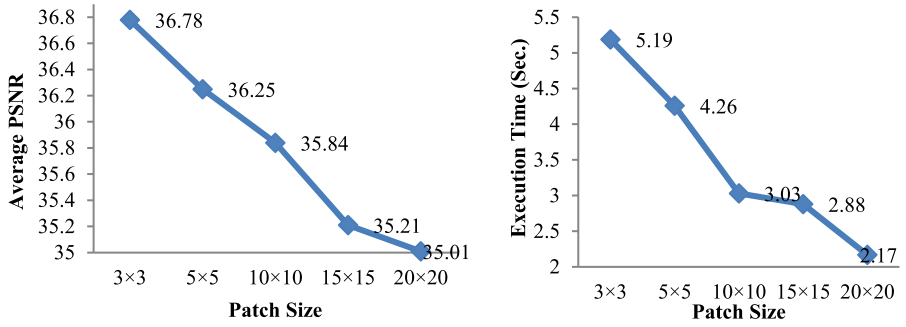

Fig. 5. Analysis of patch size a) Average PSNR vs Patch size b) Execution time vs Patch size.

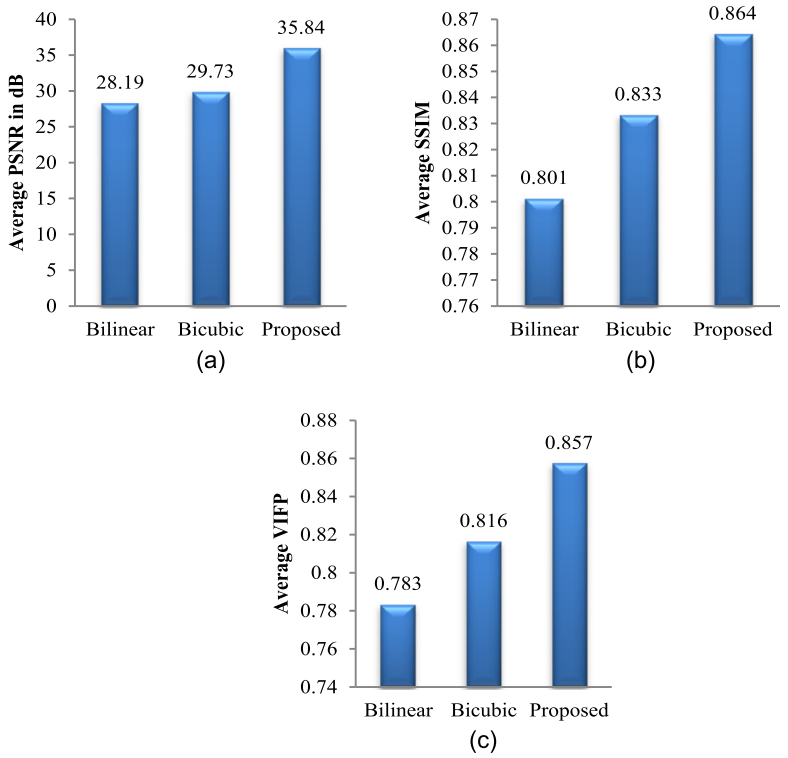

Fig. 6. Performance analysis for up-sampling factors 2 of brain images, the average (a) PSNR (b) SSIM (c) VIFP.

Table 3
Accuracy metrics in terms of accuracy, specificity, sensitivity and precision.

Class	TP	TN	FP	FN	Accuracy	Specificity	Sensitivity	Precision
No Tumor	325	572	10	7	98.14	0.982	0.9791	0.9704
Tumor	325	572	7	10	98.14	0.9879	0.9701	0.9789

Table 4
Comparison with existing approaches.

S. No.	Method	Accuracy (%)	Datasets
1	Ozyurt [38]	95.62	TCGA-GBM
2	Seetha [39]	97.5	IMAGENET
3	Afshar [40]	90.89	T1-weighed CE-MRI
4	Anaraki [41]	94.20%	T1-weighed CE-MRI
5	**Proposed Framework with ResNet-50**	**98.14**	**RIDER**

There are two types of images: Tumor and Non-tumor, as in Fig. 7 and Fig. 8.

Table 4 shows that the CNN models outperform when they are combined with the proposed system.

From Table 4, it can be seen that the proposed frameworks outperform compared to the existing methods.

4. Conclusion

This work aims to enhance the performance of brain tumor classification by using CNN methods combined with a super-resolution procedure. A novel DCT-based fusion technique aids in selecting the best blocks within frames from sequences of scanned

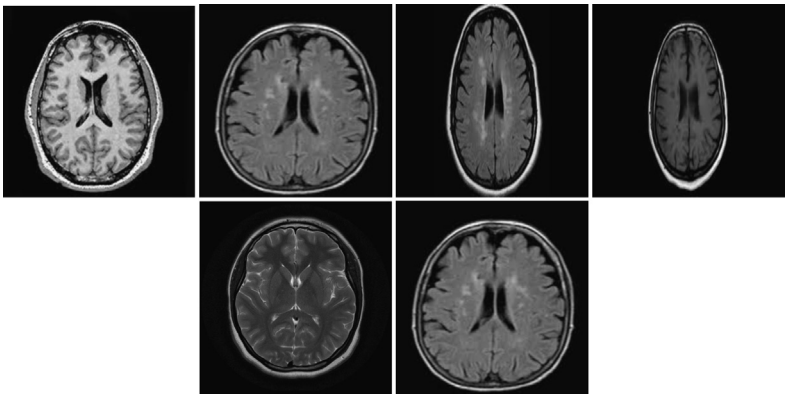

Fig. 7. No tumor images.

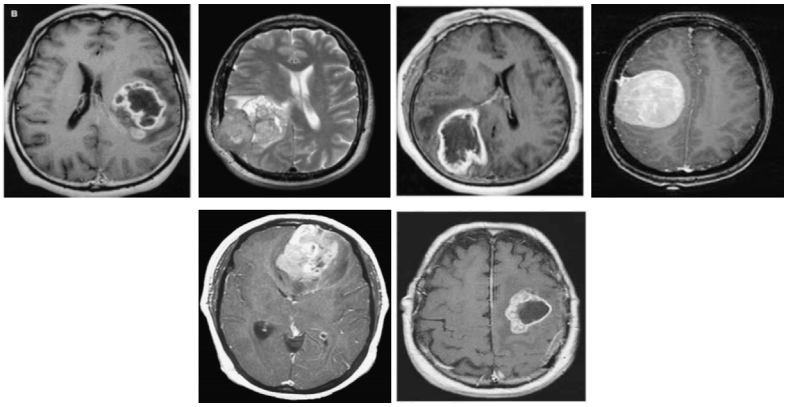

Fig. 8. Classified Tumor images.

images to fuse them. This method is termed DCT-CNN-ResNet50 and expands detail-level with the CNN-based super-resolution blocks. This strategy improves the performance of the classification system. It has been observed that the DCT-CNN-ResNet50 framework effectively super-resolves brain images and guarantees better tumor classification, especially for initial cancerous nodules and with an accuracy of 98.14% when ResNet-50 is used in the classification block.

This work is tested only for standard datasets. In future work, this method is further extended and tested for real-time scenario.

Declaration of competing interest

The authors declare that they have no known competing financial interests or personal relationships that could have appeared to influence the work reported in this paper.

References

[1] Mahmoud Khaled Abd-Ellah, Ali Ismail Awad, Ashraf A.M. Khalaf, Hesham F.A. Hamed, A review on brain tumor diagnosis from MRI images: practical implications, key achievements, and lessons learned, Magn. Reson. Imaging 61 (2019) 300–318.

[2] T. Logeswari, M. Karnan, An improved implementation of brain tumor detection using segmentation based on hierarchical self-organizing map, Int. J. Comput. Theory Eng. 2 (4) (2010) 591–598.

[3] M.K. Abd-Ellah, A.I. Awad, A.A.M. Khalaf, H.F.A. Hamed, Classification of brain tumor MRIs using a kernel support vector machine, in: Building Sustainable Health Ecosystems: 6th International Conference on Well-Being in the Information Society, WIS 2016, in: CCIS, vol. 636, 2016, pp. 151–160.

[4] Anand Deshpande, Prashant Patavardhan, Survey of super resolution techniques, ICTACT J. Image Video Proc. 9 (3) (2019).

[5] Anand Deshpande, Prashant Patavardhan, Super resolution of long range captured multiframe iris polar images, IET Biometrics 6 (5) (2017) 360–368.

[6] Anand Deshpande, Prashant Patavardhan, Multiframe super-resolution for long range captured iris polar image, IET Biometrics 6 (2) (2017) 108–116.

[7] Anand Deshpande, Navid Razmjooy, Vania V. Estrela, Introduction to computational intelligence and super-resolution, in: Computational Intelligence Methods for Super-Resolution in Image Processing Applications, 2021, pp. 3–24.

[8] Anand Deshpande, Prashant Patavardhan, Iterated back projection based super-resolution for iris feature extraction, Proc. Comput. Sci. 48 (2015).

[9] Anand Deshpande, Prashant Patavardhan, Vania V. Estrela, Super resolution and recognition of unconstrained ear image, Int. J. Biom. 12 (4) (2020).

[10] Anand Deshpande, Prashant Patavardhan, Vania V. Estrela, Deep learning as an alternative to super-resolution imaging in UAV systems, in: IET Imaging and Sensing for Unmanned Aircraft Systems, 2020.

[11] Anand Deshpande, Prashant P. Patavardhan, Super-resolution of long range captured iris image using deep convolutional network, in: IOS Deep Learning for Image Processing Applications, 2017.

[12] Anand Deshpande, Prashant Patavardhan, Unconstrained iris image super resolution in transform domain, in: Springer Networking Communication and Data Knowledge Engineering, November 2017, pp. 173–180.

[13] Anand Deshpande, Prashant Patavardhan, Feature extraction and fuzzy based feature selection methods for long range captured iris images, in: Springer Networking Communication and Data Knowledge Engineering, November 2017, pp. 137–144.

[14] E. Sert, D. Avci, Brain tumor segmentation using neutrosophic expert maximum fuzzy-sure entropy and other approaches, Biomed. Signal Process. Control 47 (2019) 276–287.

[15] F. Özyurt, E. Sert, E. Avci, E. Dogantekin, Brain tumor detection based on convolutional neural network with neutrosophic expert maximum fuzzy sure entropy, Measurement 147 (2019) 106830.

[16] M. Havaei, A. Davy, D. Warde-Farley, A. Biard, A. Courville, Y. Bengio, et al., Brain tumor segmentation with deep neural networks, Med. Image Anal. 35 (2017) 18–31.

[17] V. Rajinikanth, S.C. Satapathy, S.L. Fernandes, S. Nachiappan, Entropy based segmentation of tumor from brain MR images – a study with teaching learning based optimization, Pattern Recognit. Lett. 94 (2017) 87–95.

[18] Xiaomei Zhao, Yihong Wu, Guidong Song, Zhenye Li, Yazhuo Zhang, Yong Fan, A deep learning model integrating FCNNs and CRFs for brain tumor segmentation, Med. Image Anal. 43 (2018) 98–111.

[19] N. Tustison, K.L. Shrinidhi, M. Wintermark, C.R. Durst, B.M. Kandel, J.C. Gee, et al., Optimal symmetric multimodal templates and concatenated random forests for supervised brain tumor segmentation (simplified) with ANTsr, Neuroinformatics 13 (2015) 209–225.

[20] S. Deepak, P.M. Ameer, Brain tumor classification using deep CNN features via transfer learning, Comput. Biol. Med. 111 (2019) 103345.
[21] Zaka Ur Rehman, Syed S. Naqvi , Tariq M. Khan, Muhammad A. Khan, Tariq Bashir, Fully automated multi-parametric brain tumour segmentation using superpixel based classification, Expert Syst. Appl. 118 (2019) 598–613.
[22] Zar Nawab Khan Swati, Qinghua Zhao, Muhammad Kabir, Farman Ali, Zakir Ali, Saeed Ahmed, et al., Brain tumor classification for MR images using transfer learning and fine-tuning, Comput. Med. Imaging Graph. 75 (2019) 34–44.
[23] M.M. Badza, M.C. Barjaktarovic, Classification of brain tumors from MRI images using a convolutional neural network, Appl. Sci. 10 (6) (2020) 1–13.
[24] E. Irmak, COVID-19 disease severity assessment using CNN model, IET Image Process. (2021).
[25] H.A. Khan, W. Jue, M. Mushtaq, M.U. Mushtaq, Brain tumor classification in MRI image using convolutional neural network, Math. Biosci. Eng. 17 (5) (2020) 6203–6216, https://doi.org/10.3934/MBE.2020328.
[26] Boyina Subrahmanyeswara Rao, Dynamic histogram equalization for contrast enhancement for digital images, Appl. Soft Comput. 89 (April 2020).
[27] https://users.cs.cf.ac.uk/Dave.Marshall/Multimedia/node231.html.
[28] Yong Yang, A novel DWT based multi-focus image fusion method, Proc. Eng. 24 (2011).
[29] https://medium.com/analytics-vidhya/cnns-architectures-lenet-alexnet-vgg-googlenet-resnet-and-more-666091488df5.
[30] https://towardsdatascience.com/the-w3h-of-alexnet-vggnet-resnet-and-inception-7baaaecccc96.
[31] https://towardsdatascience.com/understanding-and-coding-a-resnet-in-keras-446d7ff84d33.
[32] D. Barboriak, Data from RIDER_NEURO_MRI, Cancer Imaging Archive, 2015.
[33] C. Navoneel, https://www.kaggle.com/navoneel/brain-mri-images-for-brain-tumor-detection.
[34] Z. Wang, A. Bovik, H. Sheikh, E. Simoncelli, Image quality assessment: from error visibility to structural similarity, IEEE Trans. Image Process. 13 (4) (2004) 600–612.
[35] H.R. Sheikh, A.S. Bovik, G. de Veciana, An information fidelity criterion for image quality assessment using natural scene statistics, IEEE Trans. Image Process. 14 (12) (2005) 2117–2128.
[36] T. Lukes, K. Fliegel, M. Klima, Performance evaluation of image quality metrics with respect to their use for super-resolution enhancement, in: Fifth International Workshop on Qualcomm Multimedia Experience, 2013.
[37] X. Zhou, B. Bhanu, Evaluating the quality of super-resolved images for face recognition, in: IEEE Computer Society Conference on Computer Vision and Pattern Recognition Workshops, 2008.
[38] A. Dogantekin, F. Ozyurt, E. Avcı, M. Koç, A novel approach for liver image classification PH-C-ELM, Measurement 137 (2019) 332–338, https://doi.org/10.1016/j.measurement.2019.01.060.
[39] J. Seetha, S.S. Raja, Brain tumor classification using convolutional neural networks, Biomed. Pharmacol. J. 11 (3) (2018) 1457–1461.
[40] P. Afshar, K.N. Plataniotis, A. Mohammadi, Capsule networks for brain tumor classification based on MRI images and coarse tumor boundaries, in: ICASSP 2019-2019 IEEE International Conference on Acoustics, Speech and Signal Processing (ICASSP), IEEE, 2019.
[41] A.K. Anaraki, M. Ayati, F. Kazemi, Magnetic resonance imaging-based brain tumor grades classification and grading via convolutional neural networks and genetic algorithms, Biocybern. Biomed. Eng. 39 (1) (2019) 63–74.